

## Article

# Comparative Analysis of Composition and Porosity of the Biogenic Powder Obtained from Wasted Crustacean Exoskeletons after Carotenoids Extraction for the Blue Bioeconomy

Fran Nekvapil <sup>1,2,3</sup> , Maria Mihet <sup>2</sup>, Geza Lazar <sup>1,3</sup>, Simona Cîntă Pinzaru <sup>1,3</sup> , Ana Gavrilović <sup>4</sup>,  
Alexandra Ciorîță <sup>2,5</sup> , Erika Levei <sup>6</sup> , Tudor Tamaş <sup>7</sup>  and Maria-Loredana Soran <sup>2,\*</sup> 

<sup>1</sup> Ioan Ursu Institute, Babeş-Bolyai University, 1 Kogălniceanu, 400084 Cluj-Napoca, Romania; fran.nekvapil@ubbcluj.ro (F.N.)

<sup>2</sup> National Institute for Research and Development of Isotopic and Molecular Technologies, 67-103 Donat, 400293 Cluj-Napoca, Romania; maria.mihet@itim-cj.ro (M.M.)

<sup>3</sup> RDI Institute of Applied Natural Sciences, Babeş-Bolyai University, Fântânele 30, 400327 Cluj-Napoca, Romania

<sup>4</sup> Faculty of Agriculture, University of Zagreb, Svetošimunska 25, 10000 Zagreb, Croatia

<sup>5</sup> Electron Microscopy Center, Babeş-Bolyai University, 5-7 Clinicilor, 400006 Cluj-Napoca, Romania

<sup>6</sup> INCDO-INOE 2000, Research Institute for Analytical Instrumentation, 67 Donat, 400296 Cluj-Napoca, Romania

<sup>7</sup> Department of Geology, Babeş-Bolyai University, 1 Kogălniceanu, 400084 Cluj-Napoca, Romania

\* Correspondence: loredana.soran@itim-cj.ro

**Abstract:** The recovery and recycling of wasted resources are at the forefront of contemporary global issues. Methods of addressing several different issues may go hand-in-hand with each other, such as linking food waste recycling into bio-based adsorbent materials and wastewater treatment. Crustacean exoskeletons are promising candidates for bio-friendly adsorbents; however, maximizing their efficiency requires the optimization of processing technology. Crustacean meat offers an (often luxury) culinary delicacy, while their waste exoskeletons offer opportunities for smart recycling of the magnesian calcite nanoporous biocomposite. Here, we conduct a structural characterization of the exoskeletons of three crustacean species to assess how the extraction of valuable carotenoids affects prospects for the further valorization of their porous powder. The exoskeleton powder's composition and morphology were investigated by SEM, Raman spectroscopy, FTIR and XRD. The biomineral component magnesian calcite was recorded both in native and in post-extraction exoskeleton powder. Acetone extraction, however, partially removed organic matter from the exoskeletons, resulting in the porosity of the respective powder increasing significantly from below  $10 \text{ m}^2 \text{ g}^{-1}$  in the native powder to over  $32 \text{ m}^2 \text{ g}^{-1}$  in post-extraction samples of blue crab and spider crab exoskeletons—while the spiny lobster exoskeleton exhibited low porosity, as measured by the BET method. This new insight could improve exoskeleton processing in the sustainable circular economy and applied blue bioeconomy—most notably for adsorbent materials for pollutants dissolved in water or as ordered, nature-derived nanostructured templates.

**Keywords:** waste exoskeletons; blue bioeconomy; structural characterization; carotenoids; porosity



**Citation:** Nekvapil, F.; Mihet, M.; Lazar, G.; Pinzaru, S.C.; Gavrilović, A.; Ciorîță, A.; Levei, E.; Tamaş, T.; Soran, M.-L. Comparative Analysis of Composition and Porosity of the Biogenic Powder Obtained from Wasted Crustacean Exoskeletons after Carotenoids Extraction for the Blue Bioeconomy. *Water* **2023**, *15*, 2591. <https://doi.org/10.3390/w15142591>

Academic Editor: Chao Yang

Received: 19 April 2023

Revised: 11 July 2023

Accepted: 13 July 2023

Published: 16 July 2023



**Copyright:** © 2023 by the authors. Licensee MDPI, Basel, Switzerland. This article is an open access article distributed under the terms and conditions of the Creative Commons Attribution (CC BY) license (<https://creativecommons.org/licenses/by/4.0/>).

## 1. Introduction

Crustacean exoskeleton powder is a likely candidate for multiple valorization pathways through the blue bioeconomy and the circular economy as a secondary raw material. Numerous studies have focused on the extraction of chitin as a valuable biomolecule with biomedical applications [1–3]. However, a new view of crustacean exoskeleton waste through the lenses of the blue bioeconomy, spearheaded by the BlueBioSustain project [4], aims to specifically exploit the value of their natural nanoscale porosity (which is difficult to create artificially beyond the laboratory scale). This biomimetic approach is in stark

contrast to the extraction of exoskeleton constituents—such as chitin for example, where biotechnological production [1] and modification [5] methods exist.

The natural porosity of mineralized structures is a widely exhibited property in biota, from planktonic organisms [6,7], echinoids [8] and avian eggs [9], to crustacean species weighing up to several kilograms [10]. In many diatoms, the organization of the pores—called alveolae, arranged in rows called striae—are one of the key features for species identification [6]. In crabs, the pores of live organisms are believed to house cellular processes that facilitate exoskeleton formation, but the ordered arrangement of surface pores may also act as a natural photonic crystal, adding a structural component to the overall shell-color aspect [10]. The porous calcified “shell” is not merely a mineral plate, but is rather created by a process called biomineralization, where calcium carbonate is deposited on an organic scaffold consisting of a wide variety of fibrous and specialized proteins to form an immensely complex multi-layered biocomposite. Exoskeletons often have stunning mechanical properties and an array of biological functions optimized through millennia of evolution [9,11].

The porous structure of crab exoskeleton parts has recently been investigated in numerous studies [10,12–16], presenting potential for innovative applications. For instance, using Raman spectroscopy techniques, Lazar et al. [13] have shown the possibility of loading nanoporous exoskeleton-derived powder with the anti-cancer drug 5-fluorouracil, and its subsequent release in aqueous solution. Another direct application of the nanoporous structure is loading with seaweed extracts [16], with subsequent usage as a biostimulant for vegetables [4].

Biogenic nanoporous materials have also attracted increasing interest in recent years in the field of adsorption science for their natural porosity and wide availability. Thus, among others, crab, shrimp, and oyster shells have also been considered [17–21]. A recent review specifically focused on the recycling of crab exoskeletons for heavy metal adsorption revealed that acid or alkaline washes are the most common processing steps for adsorbent production—sometimes also coupled with thermal treatment [22].

A facilitating aspect of such biogenic nanostructured materials is their wide availability. Various forms of waste shells can be found as refuse from seafood markets, the processing industry, and also restaurant waste. According to the worldwide datasets made available by the UN Food and Agriculture Organization [23], crustacean captures are exhibiting an increasing trend—amounting to a total of over 5.6 million tons fresh weight in 2020. Taking into account that about 52% of fresh crab mass is raw input feed for biogenic powder production [24], and supposing well-developed collection logistics, it follows that a potential 2.9 million tons of exoskeletons may be available for recycling into secondary biogenic resources. This *waste* would otherwise be destined for landfilling as common garbage, but its upcycling is not only attractive as an environmental protection issue, but is also aligned with major contemporary international strategies calling for research into opportunities for aquatic resources—bringing further funding sources for research and the private sector [25–27]. The foundation for biogenic waste management was laid more than a decade ago [28], and it is still being revised according to the newest technological solutions.

Reports on the surface area of native exoskeletons of common crab species are scant. Lazar et al. [13] recently reported the pore surface area of the Atlantic blue crab (*Callinectes sapidus*) as below  $10 \text{ m}^2 \text{ g}^{-1}$  after milling of the native carapace. Methods for the removal of the organic fraction of the exoskeleton composite may potentially increase the porosity of the resulting powder. For instance, Ogresta et al. [29] have shown that certain chemical treatments such as moderate heating in the presence of NaOH result in a decrease of the total content of organic matter in wasted exoskeletons. Enzymatic treatments of exoskeleton powder using proteolytic enzymes have also been explored for the removal of organic matter [30]. Although these methods are efficient in protein removal, porosity was not subsequently measured.

Crustacean exoskeletons also contain valuable carotenoids [30–34]. Naturally, carotenoids and carotenoproteins give specific colors to the exoskeletons, or even serve as photorecep-

tors [35]. In the current context, however, carotenoids are strong commercial antioxidants, and pairing of carotenoid extraction with adsorbent production as a subsequent step enables the maximization of exoskeleton valorization opportunities. This would result in an upcycling chain with more links, starting from the same waste exoskeleton stock—rather than processing more stocks through shorter upcycling chains. This approach is also advantageous from the logistics point of view.

The novelty of this study consists of a new approach to improve the efficiency of waste crustacean exoskeleton recycling prospects, including concomitant carotenoid extraction and the increasing of exoskeleton powder porosity. This approach holds advantages for blue biotechnology and biomimetics applications—most notably as an adsorbent material—thereby increasing the options for exoskeleton recycling.

We validated our approach by comparative structural characterization of the exoskeletons, aiming to determine how their structural properties—i.e., their morphology, chemical composition and porosity—are affected by treatment with an organic solvent, which is a step usually employed for carotenoid extraction. Three species were used to account for certain biological variations in the exoskeleton structure: the carotenoid-rich, stiff exoskeleton of the Atlantic blue crab (*C. sapidus*, the blue crab); the carotenoid-poor exoskeleton of the European spider crab (*Maja squinado*, the spider crab); and the thin, lightweight exoskeleton of the European spiny lobster (*Palinurus elephas*, the spiny lobster). We also compared the content of the extracts to find out more about the effect of contact with the solvent.

## 2. Materials and Methods

### 2.1. Materials Sourcing and Preparation

Crustacean specimens of the blue crab and spider crab were sourced in the north-eastern Adriatic Sea and were obtained from sample sets within benthic biota monitoring activities conducted periodically by Croatia state authorities for research purposes. Spiny lobster exoskeletons were obtained as seafood restaurant waste in the Dubrovnik area. All exoskeleton parts were immediately pre-processed to preserve the material during short-term storage—including short-term thermal treatment (10 min in boiling in water) to allow for the easier cleaning of soft tissue—and subsequently dried in air at 50 °C. All parts of the exoskeleton of the considered species were ground together to millimetric fragments using an electric chopper (Gorenje 450 W)—hence, the obtained results refer to the median properties of each species. Exoskeleton fragments of each species were subsequently milled to powder in an RS 200 vibratory disc mill (Retsch, Haan, Germany) with a tungsten chamber for further comparative analysis.

A subset of the ground exoskeleton fragments from each species was subjected to carotenoid extraction before milling into powder. Extraction from the fragments was carried out in acetone, in a static system, where batches of 100 g of unselected fragments of each studied species were covered with 450 mL of solvent. After 24 h of extraction, the liquid carotenoid-rich phase was decanted. The resulting carotenoid-depleted exoskeleton fragments are termed the “post-extraction” samples throughout the remainder of this paper, and they are comparatively analyzed in the powder state along with their untreated, “native” counterparts from the same species.

### 2.2. Analysis of the Extract

Fourier-Transform infrared absorption (FTIR) and Raman spectroscopy were used for the chemical characterization of the extracts. Samples for the Raman analysis were prepared by a drop-coating method on a standard glass microscope slide. Spectra were acquired after solvent evaporation using an iRaman Plus (B&W Tek, Plainsboro Township, NJ, USA) portable spectrometer coupled to a digital microscope via an optic fiber. The 532 nm laser wavelength was employed to pre-resonantly enhance the carotenoid signal. A 50x objective was used. Spectra were recorded in the 0–4000  $\text{cm}^{-1}$  range (4  $\text{cm}^{-1}$  resolution), with 10 average 10 s integration time scans, under either 6 or 30 mW laser power, depending on the intrinsic fluorescence level of the samples.

Fourier-transform infrared (FTIR) spectra were recorded using a Spectrum BX II (Perkin-Elmer, Waltham, MA, USA) with an ATR accessory kit. The precipitate was analyzed after solvent evaporation on the sampling window in the 600–4000  $\text{cm}^{-1}$  range, with 32 scans.

### 2.3. Analysis of Native and Post-Extraction Exoskeleton Powders

The nanomorphology of the bulk fragments was imaged by a Hitachi SU8320 cold field emission scanning electron microscope (Hitachi, Tokyo, Japan) to provide an overview of the studied materials. Samples were placed on a stub holder and sputter-covered with a 10 nm-thick layer of gold to prevent samples melting under the electron beam. Samples were imaged under a 30 kV acceleration current.

The specific surface area, pore volume, and pore size distribution of the crustacean samples were estimated by  $\text{N}_2$  sorption analysis performed at 77 K (Sorptomatic 1990, Thermo Electron, Waltham, MA, USA). Pretreatment of the samples consisted in degassing at 150 °C under vacuum for 4 h (2 °C/min). The specific surface area was estimated according to the standard BET procedure (0.01–0.2 p/p<sub>0</sub>), while the total pore volume was estimated using the Dollimore–Heal method for the desorption branch.

Raman spectra from the powder were recorded using a Prominence handheld spectrometer (Rigaku, Tokyo, Japan) with an integrated 1064 nm excitation, recording in the 200–2000  $\text{cm}^{-1}$  range with a size-adjustable sample vial holder.

FTIR was conducted on the Perkin–Elmer spectrometer mentioned above; however, the exoskeleton powder was embedded in KBr pellets (1% by mass). Measurements were performed in the 400–4000  $\text{cm}^{-1}$  range with 4 scans under a 1  $\text{cm}^{-1}$  resolution.

X-ray powder diffraction: Exoskeleton fragments were finely ground with an agate mortar and their mineral composition was verified by X-ray powder diffraction (XRPD) using a Bruker D8 Advance diffractometer in Bragg–Brentano geometry, with a Cu tube with  $\lambda_{\text{K}} = 0.15418$  nm, a Ni filter and a LynxEye detector. Corundum (NIST SRM1976a) was used as the internal standard. The data were collected on a 10–70° 2 $\theta$  interval at a 0.02° 2 $\theta$  step, measuring each step for 0.5 s. Identification of mineral phases was performed using Difrac.Eva 2.1

## 3. Results

### 3.1. Characterization of the Extracts

The Raman and FTIR spectra recorded from the exoskeleton extract of the three considered species are shown in Figure 1. Resonance Raman spectra under 532 nm excitation showed strong resonance signals for the carotenoids, with the main bands at 955  $\text{cm}^{-1}$  termed  $\nu_4$ , 1000  $\text{cm}^{-1}$  termed  $\nu_3$ , 1152  $\text{cm}^{-1}$  termed  $\nu_2$  and 1515  $\text{cm}^{-1}$  termed  $\nu_1$  (Figure 1a). These bands correspond to atomic vibrations (C–C) stretching, overlapping with  $\text{CH}_2$  and  $\text{CH}_3$  rocking, C– $\text{CH}_3$  rocking, C–C single bond stretching and C=C double bond stretching modes. Astaxanthin is an orange-to-red carotenoid that has been detected previously in blue crab and spiny lobster exoskeletons—more specifically in exocuticles up to a 20–100  $\mu\text{m}$  depth [10,35]. Our recorded bands corresponded well to the solid state astaxanthin prepared in a similar manner (drop-coating from acetone solution). However, the small variation of the C=C band shape, which is very sensitive to carotenoids' conjugated polyene chain configuration, indicated the presence of other carotenoids in our extracts as well. Carotenoid overtones were also observed in the 2000–3100  $\text{cm}^{-1}$  range—namely at 2155  $\text{cm}^{-1}$ , corresponding to the  $\nu_2 + \nu_3$  overtone; at 2304  $\text{cm}^{-1}$ , corresponding to  $2\nu_2$ ; at 2661  $\text{cm}^{-1}$  from  $\nu_1 + \nu_2$ ; and at 3022  $\text{cm}^{-1}$  from  $2\nu_1$ . Detailed assignments of all Raman-active bands of carotenoids highlighting the C=C band shifting in correlation with the carotenoid configuration can be found in our previous works focusing on  $\beta$ -carotene [36], astaxanthin [10] and fucoxanthin [37].

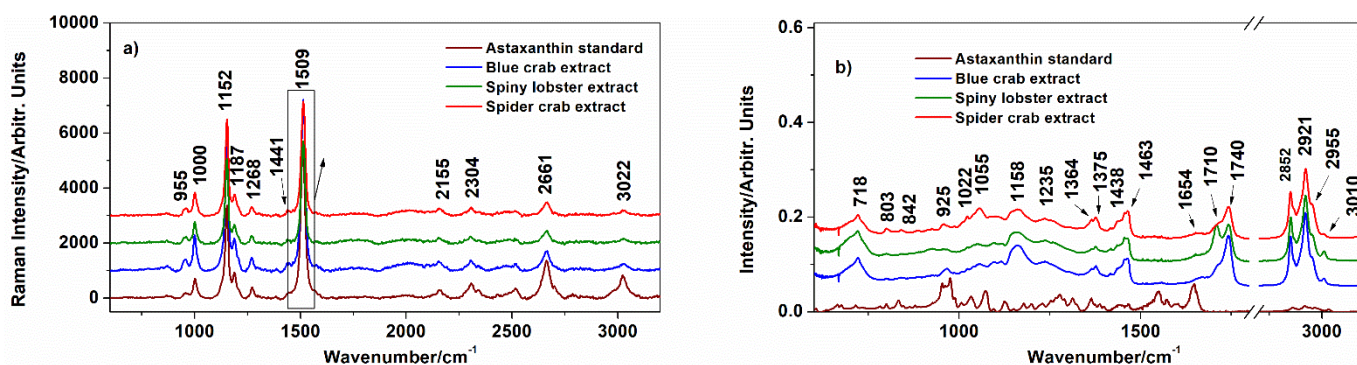


**Figure 1.** (a) Raman spectra recorded from acetone extracts of blue crab (*Callinectes sapidus*), spider crab (*Maja squinado*) and spiny lobster (*Palinurus elephas*) unselected exoskeleton fragments. Spectra are normalized to the  $\nu_1$  (C=C) band at  $1515\text{ cm}^{-1}$ , excitation =  $532\text{ nm}$ ; (b) shows the FTIR spectra of the precipitated extracts after solvent evaporation. Respective spectrum of all-*trans* astaxanthin (CAS 472-41-7) is given as reference in (a,b). All spectra are background-subtracted and y-offset was applied to both (a,b) for clarity.

FTIR showed, however, prominent signals for lipids in all extracts (Figure 1b). The characteristic absorption features of lipid are a band pair corresponding to the carboxylate group in the  $1710\text{--}1740\text{ cm}^{-1}$  range and sharp C–H stretching modes in the  $2800\text{--}3100\text{ cm}^{-1}$  range [38]. Lipid bands were not recorded in exoskeleton powder by FTIR or Raman spectroscopy (discussed below); however, it is possible that they were embedded within the organic matrix in smaller quantities and subsequently extracted by acetone. Although the scope here is not to precisely determine the fatty acid profiles, we did observe that the exoskeletons of different crustacean species contained slightly different fatty acid compositions. This is clearly visible by the variation of the  $1710$  to  $1740\text{ cm}^{-1}$  bands ratio, meaning that the spiny lobster exoskeleton contained the highest proportion of free fatty acids relative to esters. The bands in the  $1300\text{--}1490\text{ cm}^{-1}$  range are broadly assigned to C–H bending modes, those in  $1000\text{--}1300\text{ cm}^{-1}$  to C–O stretching modes, while those at lower wavenumbers are assigned to skeletal modes involving -HC=CH- moieties [38]. A detailed discussion on the FTIR features of lipids is presented in a paper by Guillén and Cabo [38].

### 3.2. Exoskeleton Ultrastructure

The nanoporous structure of the native and post-extraction bulk blue crab exoskeletons is shown in Figure 2a,b, along with their visual aspects in Figure 2c,d. The well-described pores and channels were also observed here, with pore diameters of around  $50$  to  $70\text{ nm}$ —as previously reported for blue crabs sampled in another region, the southern Adriatic Sea [10] and exoskeletons of some other crab species [15,35]. According to the data published on similar materials, mechanical milling of the exoskeleton fragments resulted in powder with a wide particle size distribution spanning from  $<1$  to  $>250\text{ }\mu\text{m}$ , but with the majority of particles within the  $1$  to  $50\text{ }\mu\text{m}$  class [12,29].

### 3.3. Exoskeleton Powder Porosity

BET measurements evidence the mesoporous structure of the native and especially the post-extraction exoskeleton powder. All samples showed type IV isotherms according to the IUPAC classification [39] (isotherms shown in Supplementary Materials Figure S1). Additionally, an increase in both surface area and pore volume as a consequence of the carotenoid extraction procedure for all the investigated powder samples can be noticed (Table 1). The surface area increased four times in the case of the blue crab exoskeleton powder, and ten times for the spider crab powder, reaching values around  $32\text{ m}^2\text{ g}^{-1}$ . The post-extraction spiny lobster exoskeleton powder showed a much lower surface area—that is,  $1.4\text{ m}^2\text{ g}^{-1}$ ; however, this is notable as compared to the native sample, which showed

no measurable surface area. Moreover, the extraction procedure allowed the exposure of pores in the mesoporous domain (2–50 nm) in the case of all samples, which led to an enhancement of total pore volume of at least 2.5 times (Table 1). In respect to the pore size distribution—for the same crustacean species—both the native and the post-extraction powders showed a wide and similar distribution, with pore dimensions ranging from 5 to 50 nm.

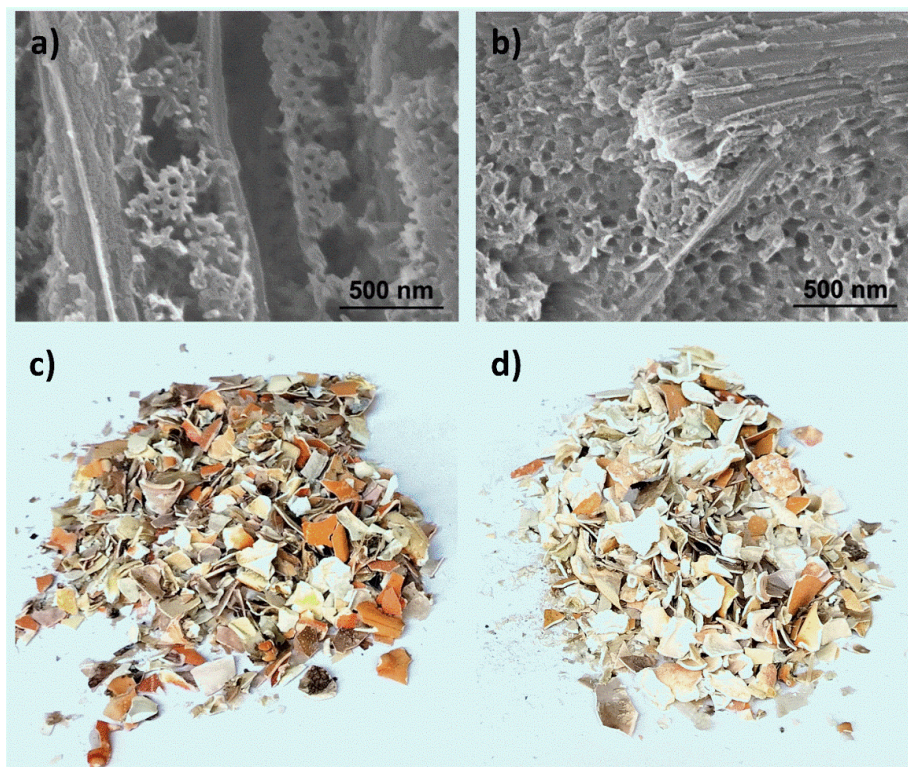


**Figure 2.** SEM images of the blue crab (*Callinectes sapidus*) exoskeleton fragments in their native state (a) and after carotenoid extraction (b), and the respective photographs of native and post-extraction exoskeleton waste in (c,d), respectively.

**Table 1.** Textural properties of native and post-extraction exoskeleton powder of the blue crab, the spider crab and the spiny lobster, according to the BET method.

Sample, Treatment	Specific Surface Area ( $\text{m}^2 \text{g}^{-1}$ )	Pore Volume ( $\text{cm}^3 \text{g}^{-1}$ )
Blue crab exoskeleton powder, native	8.2	0.049
Blue crab exoskeleton powder, post-extraction	32.9	0.135
Spider crab exoskeleton powder, native	3.2	0.051
Spider crab exoskeleton powder, post-extraction	32.6	0.138
Spiny lobster exoskeleton powder, native	0	0.012
Spiny lobster exoskeleton powder, post-extraction	1.4	0.030

### 3.4. Exoskeleton Powder Chemical Composition

The native crustacean exoskeletons considered here were characterized through Raman spectroscopy (Figure 3), FTIR (Figure 4), and XRD (Figure 5). In Raman spectra, calcite is represented in all samples by the bands at 280–281, 713 and 1087  $\text{cm}^{-1}$  [40], and the presence of monohydrocalcite in the spiny lobster exoskeleton (Figure 3c) is indicated by the band at 1067  $\text{cm}^{-1}$ . Monohydrocalcite is a  $\text{CaCO}_3$  polymorph not usually reported in the 33s of living invertebrates; however, this phase has been observed to form in crab exoskeleton stocks under certain environmental or storage conditions—possibly through an abiotic process [29]. Another important compound detected in all powder samples was

chitin, a natural polymer constituting the organic scaffold of exoskeletons, represented by numerous wide bands in the 300–600  $\text{cm}^{-1}$  range and bands at 895, 953, 1162, 1203, 1264, 1325, 1374, 1451 and 1664  $\text{cm}^{-1}$  [41]. The oddly-shaped feature around 891  $\text{cm}^{-1}$  in the spectra of the spiny lobster exoskeleton (Figure 3c) powder was presumably an instrumental artefact promoted by the extreme fluorescence background signal arising from the high organic content of the sample. The assignment of Raman bands following the published literature is given in Table 2 to the greatest confidence level of detail.

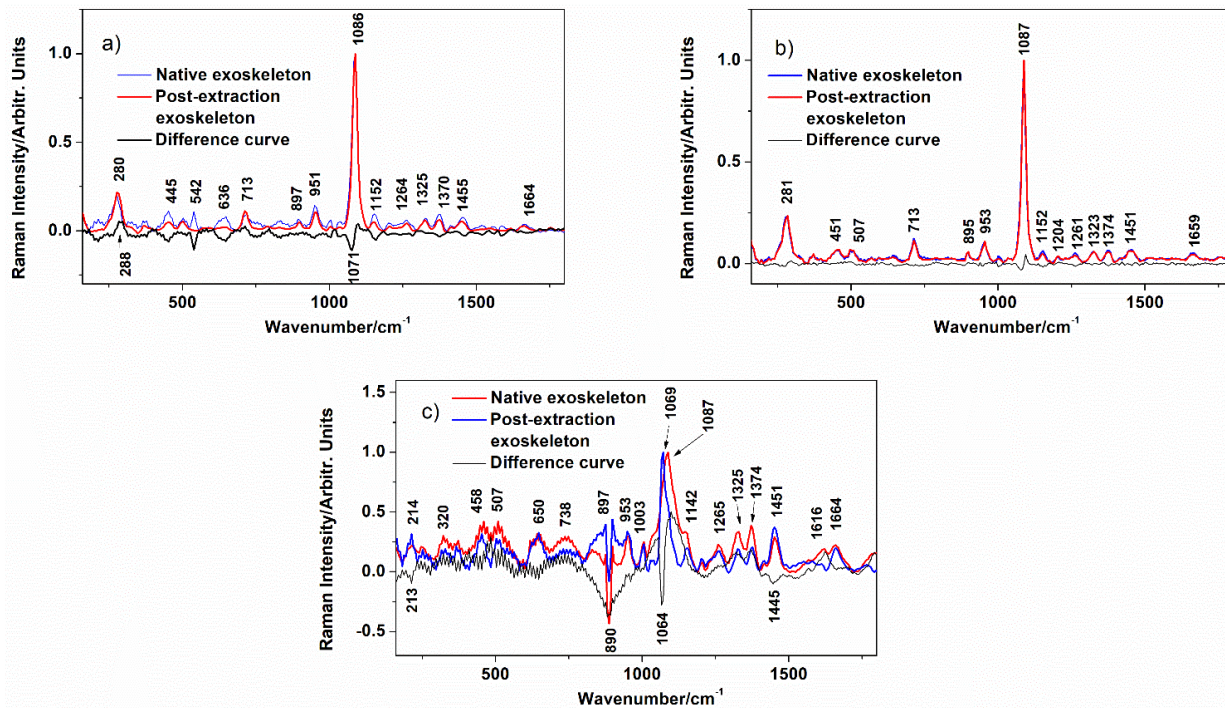


**Figure 3.** Raman spectra recorded from the (a) blue crab (*Callinectes sapidus*), (b) spider crab (*Maja squinado*) and (c) spiny lobster (*Palinurus elephas*) exoskeleton powder. Excitation = 1064 nm. Spectra are baseline-subtracted and normalized to the  $\text{CO}_3^{2-}$  band at 1087  $\text{cm}^{-1}$ .

**Table 2.** Assignments for the main Raman bands according to references [40,41] recorded in the native exoskeleton powder of the blue crab (*Callinectes sapidus*), the spider crab (*Maja squinado*) and the spiny lobster (*Palinurus elephas*). MHC = monohydrocalcite.

Band Position/ $\text{cm}^{-1}$			
Blue Crab	Spider Crab	Spiny Lobster	Assignment
280	281		L (libration) $\text{CaCO}_3$
300–600	300–600	300–600	chitin skeletal chains
713	713		$V_4(\text{CO}_3^{2-})$ in-plane bending
892	895	897	chitin skeletal chain
951	953	953	Chitin
		1003	protein trace
		1069	$\nu_{1 \text{ symm}}(\text{CO}_3^{2-})$ MHC
1086	1087	1087	$\nu_{1 \text{ symm}}(\text{CO}_3^{2-})$ calcite
1152	1152	1142	chitin
	1204		chitin
1264	1261	1265	$\rho(\text{C-H})$ chitin
1325	1323	1325	$\rho(\text{C-H})$ chitin
1370	1374	1374	$\rho(\text{C-H})$ chitin
1455	1451	1451	$\rho(\text{C-H})$ chitin
		1616	Chitin
1664	1659	1664	Amide I of chitin

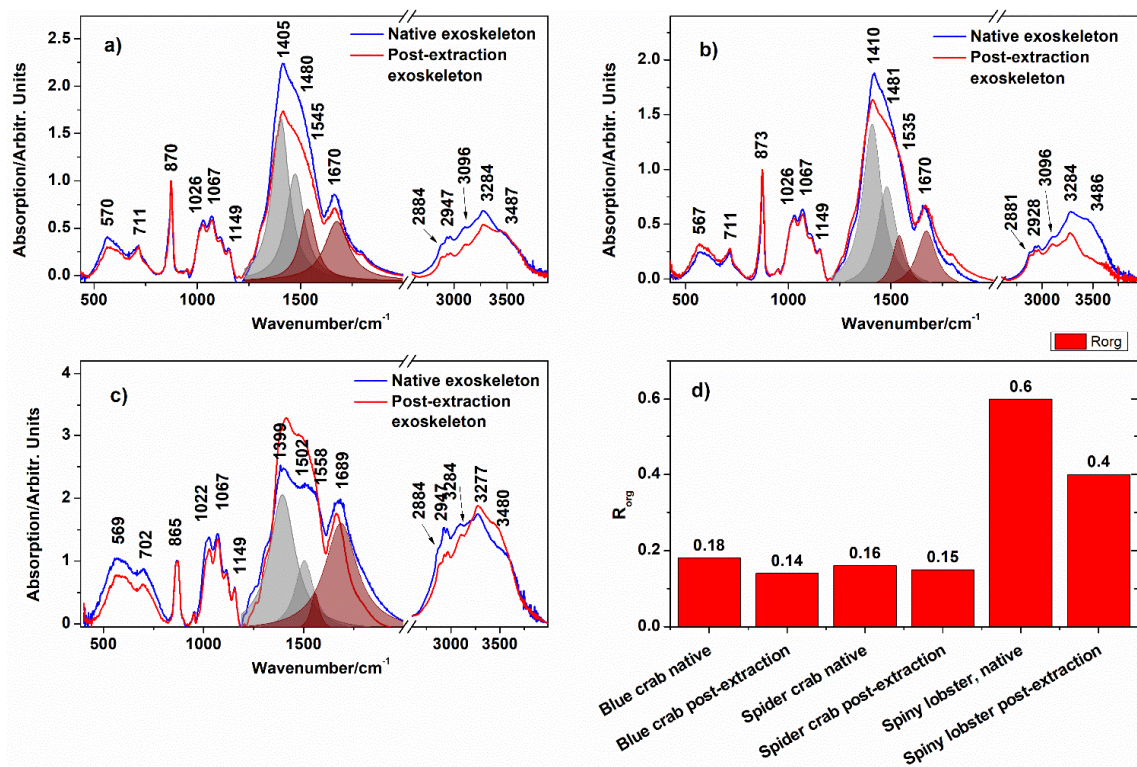


**Figure 4.** FTIR spectra recorded from the (a) blue crab (*Callinectes sapidus*), (b) spider crab (*Maja squinado*) and (c) spiny lobster (*Palinurus elephas*) exoskeleton powder. Spectra are baseline-subtracted and normalized to the CO<sub>3</sub><sup>2-</sup> band around 1400 cm<sup>-1</sup>. Deconvoluted gray-shaded Lorentzian bands represent carbonate vibrational modes, while red-shaded Lorentzian bands represent organic matter modes. Component (d) shows the relative organic matter content of the powder.

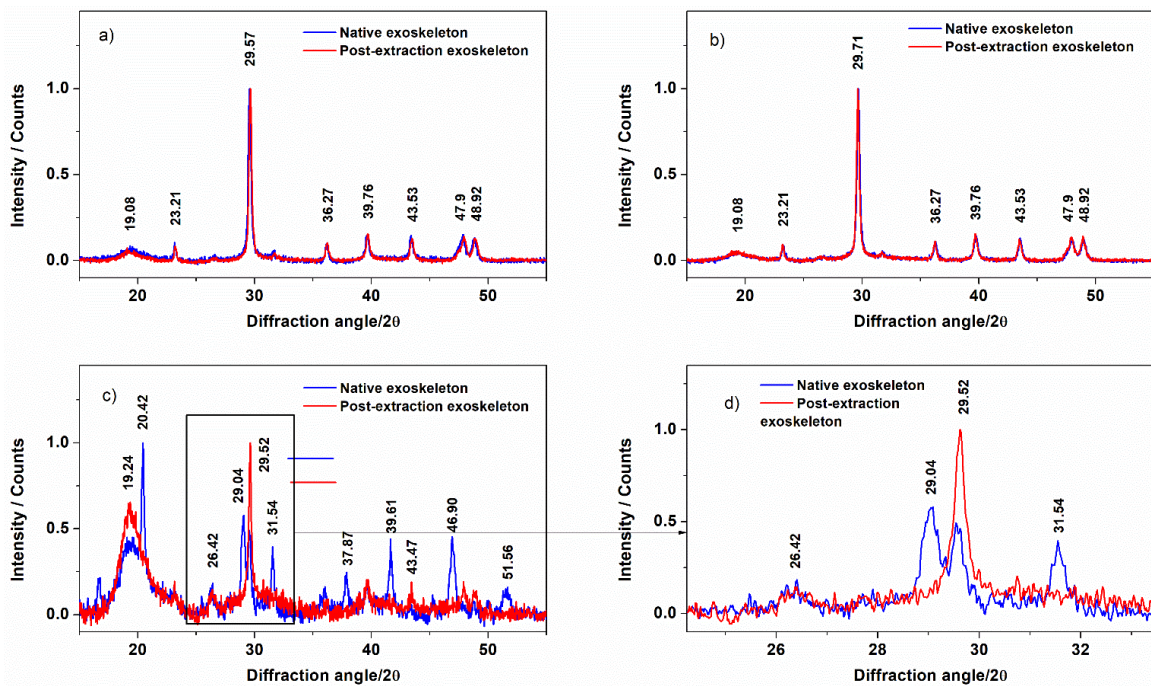


**Figure 5.** XRD patterns recorded from the (a) blue crab (*Callinectes sapidus*), (b) spider crab (*Maja squinado*), and (c) spiny lobster (*Palinurus elephas*) exoskeleton powder. Spectra are baseline-subtracted. Component (d) shows a zoom of the 25–33° 2θ range from the spiny lobster patterns, where the strongest reflection peaks for Mg-calcite and monohydrocalcite appear.

In order to enable quantitative comparison, all spectra were normalized to the carbonate stretching mode  $\nu_1$  ( $\text{CO}_3^{2-}$ ) at around  $1087\text{ cm}^{-1}$ . Difference curves were obtained by the subtraction of the Raman spectra acquired from the native powder from those acquired from the post-extraction powder under  $1064\text{ nm}$  excitation. The negative band in the difference curve at  $1071\text{ cm}^{-1}$  indicates that the native blue crab (Figure 3a) stock considered here may have contained smaller amounts of amorphous  $\text{CaCO}_3$  and monohydrocalcite than reported earlier in similar samples [29], which was eliminated in post-extraction exoskeleton fragments. The spider crab exoskeleton powder showed almost no difference before and after carotenoid extraction (Figure 3b). In the spiny lobster, however, the abundant monohydrocalcite from the native exoskeleton ( $\nu_1$  band at  $1069\text{ cm}^{-1}$ ) transitioned to Mg-calcite ( $\nu_1$  at  $1087\text{ cm}^{-1}$ ) after acetone immersion (Figure 3c). According to the current comparison method, the organic component of the spiny lobster exoskeleton also suffered modifications, with negative peaks at  $897$  and  $1445\text{ cm}^{-1}$ , but also positive peaks at  $1265$ ,  $1326$  and  $1374\text{ cm}^{-1}$  indicating the removal of certain moieties in the first case and increases in the chitin signal in the latter case.

The bulk Mg-calcite biomineral phase was revealed in all samples by the FTIR bands at  $686$ ,  $865$  and  $1399$ – $1410\text{ cm}^{-1}$  (Figure 4). The  $\text{CO}_3^{2-}$  asymmetric stretching mode was also observed at  $1480$ – $1492\text{ cm}^{-1}$  upon deconvolution of the complex feature in the  $1200$ – $1800\text{ cm}^{-1}$  range ( $R^2 > 0.994$ ). The latter band, together with the feature at  $567$ – $570\text{ cm}^{-1}$ , confirmed the presence of monohydrocalcite [29]. Assignments of major bands are given in Table 3 to the greatest confidence level of detail.

**Table 3.** Assignments for the main FTIR bands according to references [42–44] recorded in the native exoskeleton powder of the blue crab (*Callinectes sapidus*), the spider crab (*Maja squinado*) and the spiny lobster (*Palinurus elephas*). Band positions reported in a previous study from a mixed blue crab and Mediterranean green crab (*Carcinus aestuarii*) from the south Adriatic Sea are also given [29]. MHC = monohydrocalcite, ACC = amorphous calcium carbonate.

Band Position/ $\text{cm}^{-1}$				
Blue Crab	Spider Crab	Spiny Lobster	Ogresta et al. [29]	Assignment
582	569	561	576	MHC (lattice water)
707	714	696	700, 714	$\nu_{4b}(\text{CO}_3^{2-})$ out-of-plane bending
873	873	866	864	$\nu_{2\text{ asymm}}(\text{CO}_3^{2-})$ calcite + HMC; $\delta(\text{C-H})$ chitin
1029	1029	1026	1026	C–O asym. stretch in the phase ring
1067	1067	1067	1068	$\nu_1(\text{CO}_3^{2-})$ MHC; $\text{CH}_2\text{CO}$ stretch chitin
1149	1149	1149	1154	asym. bridge oxygen stretching
1405	1402	1399	1414	$\nu_{3b\text{ asym}}(\text{CO}_3^{2-})$ calcite + MHC + ACC
1480	1482	1492	1472	$\nu_{\text{asym}}(\text{CO}_3^{2-})$ MHC
1670	1682	1682	1662	Amide I of chitin
2884	2881	2884		$\nu(\text{CH}_{2,3})$
2957	2964	2960		$\nu_{\text{symm}}(\text{CH}_{2,3})$
3096	3096	3096		$\nu(\text{CH}_{2,3})$
3279	3282	3276	3272	$\nu(\text{NH})$ chitin $\nu(\text{O-H})$ MHC (structural water)
3487	3486	3480	3436	$\nu(\text{O-H})$ MHC (structural water)

In a previous paper [29], we cross-validated FTIR as a rapid and comprehensive method for the assessment of both biomineral and organic constituents of crab exoskeleton powder from harvested exoskeleton waste originating from South Adriatic shore crustacean capture. The relative fraction of organic matter within the exoskeleton powders was determined here through the ratio of the  $\nu(\text{CH}_{2,3})$  feature at  $2928$ – $2947\text{ cm}^{-1}$ , representing the overall organic matter, and the  $\nu_{\text{asym}}(\text{CO}_3^{2-})$  at  $1399$ – $1410\text{ cm}^{-1}$ , following the method from the above cited study— $R_{\text{org}} = I_{\text{CH}_{2,3}}/I_{\text{CO}_3}$ . Hence, the native exoskeleton of the spider crab contained the lowest fraction of organic matter, while this fraction was the highest in the spiny lobster, according to the FTIR signal (Figure 4). Acetone immersion resulted in a

reduction in organic matter fraction in all samples, resulting in a cca. 6.3 to 33% reduction in  $R_{org}$  in the post-extraction exoskeleton powders relative to the native ones.

X-ray diffraction also revealed Mg-calcite (reflection peaks at 23.21, 29.57, 36.27, 39.70, 43.57, 47.9 and 48.92° 2 $\theta$ ; PDF 01-086-2335) and  $\alpha$ -chitin (19.08–19.24° 2 $\theta$ ; PDF 00-0351974) in the blue crab (Figure 5a) and the spider crab (Figure 5b) native and post-extraction exoskeleton powders. This technique clearly revealed an increase in the characteristic Mg-calcite reflection peak at 29.52° 2 $\theta$  and the concomitant disappearance of the monohydrocalcite peaks at 29.04 and 31.54° 2 $\theta$  (PDF 00-029-0306) in the spiny lobster post-extraction exoskeleton powder compared to the native one (Figure 5c,d). The reflection peak at 25.31° 2 $\theta$  was assigned to aragonite by the PDF (2012) database (PDF 00-003-0405); however, it is very unlikely that this CaCO<sub>3</sub> polymorph would be found in spiny lobsters in natural conditions, and hence, we presume with caution that it was either an assignment error or indeed that the aragonite formed due to specific treatment conditions.

#### 4. Discussion

As shown by the results above, acetone immersion used for carotenoid extraction has a magnification effect upon the surface area and pore volume in blue crab and the spider crab exoskeleton powder. The carotenoid extraction step enhanced the overall valorization potential for the exoskeletons within the blue bioeconomy. However, natural, ordered exoskeleton porosity on the nanoscale has further implications; most notably, related properties such as the exoskeleton powder's adsorption capacity towards pollutants and other materials and its natural photonic crystal structure.

Dotto et al. [45] have indicated several key features that constitute a great and sustainable adsorbent material for water treatments. Our crab exoskeleton waste adsorbent checks off several of these traits, and hence holds potential for such an application. According to the authors [31], the cost of adsorbent production accounts for up to 70% of total water treatment costs. Adsorbent production from wasted exoskeletons could be advantageous from an economic perspective, given that the nanoporous Mg-calcite biomineral with chitin fibers is naturally pre-synthesized. The costs in this case refer to the logistics of exoskeleton collection, washing and milling. Carotenoid extraction, owing to their value, should rather be counted among the opportunities than among the costs.

Recently, Lazar et al. [13] demonstrated innovative recycling of blue crab exoskeleton nanoporosity as a novel drug carrier for the anticancer drug 5-fluorouracil. The powder is loaded with the drug and dried, while the cavities between the rough particles preserve the 5-fluorouracil during pelleting and storage. A slow-release process is expected upon dissipation of the pastille in the stomach of patients. In the respective study, native blue crab exoskeleton powder was used, with a surface area of around 7 m<sup>2</sup> g<sup>-1</sup>.

The influence of porosity enhancement on the photonic properties of exoskeletons may also be debated. Nekvapil et al. [10] has evidenced that the pores and canals, which are ordered—both with respect to their consistent diameter and their spacing—are specific to, and different among, the blue, red, and white exoskeletons of the blue crab exoskeleton. An interesting topic for future work could comprise an examination of if the presented manner of changing the porosity affects the exoskeleton's photonic properties.

Another interesting approach for exploitation is using the carapace as a template for nanostructured battery electrodes [46]. In the cited study, researchers coated the nanoporous array with a thin layer of carbon, loaded the active substances (sulfur and silicon), and finally dissolved away the CaCO<sub>3</sub> template. The increased inner surface area of the nanocanals would be advantageous for the deposition of larger amounts of active material, while the larger inner pore volume would be able to accommodate volume changes in the active materials during charge and discharge [46].

Waste management and potable water pollution are one of the major current global problems [22]. In order to divert any kind of waste 66s from landfill destinations, effective alternative processing and valorization methods must be put in place. Here, we presented a technological improvement in the quantitative characteristics of exoskeleton powder

porosity, which may be applied for improved adsorbent production with added benefits (extra valuable carotenoids [47] can be co-obtained). Further technical improvements in the absorption capability and testing of biogenic exoskeleton powder in various environments are underway by our team.

## 5. Conclusions

This study shows that the porosity of blue crab and spider crab exoskeleton powder increases several-fold during carotenoid extraction in acetone. Spiny lobster exoskeletons, however, show the lowest porosity values in the mesopore range, as measured by the BET method. This enhancement of both surface area and pore volume could be due to the co-extraction of lipids from the 66, liberating in this way the pores' interior. Structural characterization showed the transition of any monohydrocalcite that may have been present in native exoskeleton to Mg-calcite in all tested crustacean species, while no notable change in the signal of chitin was observed. The results on porosity may improve prospects for the biomimetic valorization of waste crustacean exoskeletons as an adsorbent powder and nature-derived nanotemplate. The recycling of these waste materials for adsorbent preparation could be successfully employed for blue bioeconomy purposes due to their unique physical properties and their rapid and low-cost processing.

**Supplementary Materials:** The following supporting information can be downloaded at: <https://www.mdpi.com/article/10.3390/w15142591/s1>, Figure S1: N<sub>2</sub> adsorption-desorption isotherms of the native and post-extraction blue crab (*Callinectes sapidus*), spider crab (*Maja squinado*), and spiny lobster (*Palinurus elephas*) exoskeleton powder.

**Author Contributions:** F.N. Formal Analysis, Data Curation, Project Administration, Funding Acquisition, Writing—Original Draft Preparation; M.M. Formal Analysis, Data Curation; G.L. Formal Analysis, Data Curation; S.C.P. Supervision, Validation, Writing—Review and Editing; A.G. Resources, Data Curation; A.C. Formal Investigation, Data Curation; E.L. Formal Investigation, Data Curation; T.T. Formal analysis, Data Curation; M.-L.S. Conceptualization, Methodology, Supervision, Funding Acquisition. All authors have read and agreed to the published version of the manuscript.

**Funding:** This work was supported by a grant from the Ministry of Research, Innovation and Digitalization, CNCS-UEFISCDI, project number PN-III-P1-1.1-PD-2021-0477, within PNCDI III.

**Data Availability Statement:** The data are available on request from the first or corresponding author.

**Conflicts of Interest:** The authors declare no conflict of interest.

## References

1. Elleh-Ali-Komi, D.; Hamblin, M. Chitin and Chitosan: Production and Application of Versatile Biomedical Nanomaterials. *Int. J. Adv. Sci. (Indore)* **2017**, *4*, 411–427.
2. Azuma, K.; Ifuku, S.; Osaki, T.; Okamoto, Y.; Minami, S. Preparation and Biomedical Applications of Chitin and Chitosan Nanofibers. *J. Biomed. Nanotechnol.* **2014**, *10*, 2891–2920. [[CrossRef](#)] [[PubMed](#)]
3. Aneesh, P.A.; Anandan, R.; Kumar, L.R.G.; Ajeeshkumar, K.K.; Kumar, K.A.; Mathew, S. A step to shell biorefinery—Extraction of astaxanthin-rich oil, protein, chitin, and chitosan from shrimp processing waste. *Biomass- Convers. Biorefinery* **2020**, *13*, 205–214. [[CrossRef](#)]
4. The BlueBioSustain Project. Available online: <https://bluebiosustain.granturi.ubbcluj.ro/index.html> (accessed on 3 January 2023).
5. Sajid, M.A.; Shahzad, S.A.; Hussain, F.; Skene, W.G.; Khan, Z.A.; Yar, M. Synthetic modifications of chitin and chitosan as multipurpose biopolymers: A review. *Synth. Commun.* **2018**, *48*, 1893–1908. [[CrossRef](#)]
6. Trobajo, R.; Rovira, L.; Ector, L.; Wetzel, C.E.; Kelly, M.; Mann, D.G. Morphology and identity of some ecologically important small *Nitzschia* species. *Diatom Res.* **2012**, *28*, 37–59. [[CrossRef](#)]
7. Weinkauff, M.F.G.; Zwick, M.M.; Kučera, M. Constraining the Role of Shell Porosity in the Regulation of Shell Calcification Intensity in the Modern Planktonic Foraminifer *Orbulina Universa* d'Orbigny. *J. Foraminifer. Res.* **2020**, *50*, 195–203. [[CrossRef](#)]
8. Lauer, C.; Sillmann, K.; Haussmann, S.; Nickel, K.G. Strength, elasticity and the limits of energy dissipation in two related sea urchin spines with biomimetic potential. *Bioinspiration Biomim.* **2018**, *14*, 016018. [[CrossRef](#)]
9. Gautron, J.; Stapane, L.; Le Roy, N.; Nys, Y.; Rodriguez-Navarro, A.B.; Hincke, M.T. Avian eggshell biomineralization: An update on its structure, mineralogy and protein tool kit. *BMC Cell Biol.* **2021**, *22*, 11. [[CrossRef](#)]
10. Nekvapil, F.; Pinzaru, S.C.; Barbu-Tudoran, L.; Suci, M.; Glamuzina, B.; Tamas, T.; Chiş, V. Color-specific porosity in double pigmented natural 3d-nanoarchitectures of blue crab shell. *Sci. Rep.* **2020**, *10*, 3019. [[CrossRef](#)]

11. Bentov, S.; Abehsera, S.; Sagi, A. Chapter 5: The Mineralized Exoskeletons of Crustaceans. In *Extracellular Composite Matrices in Arthropods*; Cohen, E., Moussian, B., Eds.; Springer: New York, NY, USA, 2016; pp. 137–163.
12. Nekvapil, F.; Aluas, M.; Barbu-Tudoran, L.; Suci, M.; Bortnic, R.-A.; Glamuzina, B.; Cintă Pinzaru, S. From Blue Bioeconomy toward Circular Economy through High-Sensitivity Analytical Research on Waste Blue Crab Shells. *ACS Sustain. Chem. Eng.* **2019**, *7*, 16820–16827. [[CrossRef](#)]
13. Lazar, G.; Nekvapil, F.; Hirian, R.; Glamuzina, B.; Tamas, T.; Barbu-Tudoran, L.; Pinzaru, S.C. Novel Drug Carrier: 5-Fluorouracil Formulation in Nanoporous Biogenic Mg-calcite from Blue Crab Shells—Proof of Concept. *ACS Omega* **2021**, *6*, 27781–27790. [[CrossRef](#)] [[PubMed](#)]
14. Raabe, D.; Sachs, C.; Romano, P. The crustacean exoskeleton as an example of a structurally and mechanically graded biological nanocomposite material. *Acta Mater.* **2005**, *53*, 4281–4292. [[CrossRef](#)]
15. Romano, P.; Fabritius, H.-O.; Raabe, D. The exoskeleton of the lobster *Homarus americanus* as an example of a smart anisotropic biological material. *Acta Biomater.* **2007**, *3*, 301–309. [[CrossRef](#)]
16. Nekvapil, F.; Ganea, I.-V.; Ciorîță, A.; Hirian, R.; Tomšić, S.; Martonos, I.; Pinzaru, S.C. A New Biofertilizer Formulation with Enriched Nutrients Content from Wasted Algal Biomass Extracts Incorporated in Biogenic Powders. *Sustainability* **2021**, *13*, 8777. [[CrossRef](#)]
17. Morris, A.; Sneddon, J. Use of Crustacean Shells for Uptake and Removal of Metal Ions in Solution. *Appl. Spectrosc. Rev.* **2011**, *46*, 242–250. [[CrossRef](#)]
18. Fabbicino, M.; Pontoni, L. Use of non-treated shrimp-shells for textile dye removal from wastewater. *J. Environ. Chem. Eng.* **2016**, *4*, 4100–4106. [[CrossRef](#)]
19. Rissouli, L.; Beenicha, M.; Chafik, T.; Chabbi, M. Decontamination of water polluted with pesticide using biopolymers: Adsorption of glyphosate by chitin and chitosan. *J. Mater. Environ. Sci.* **2017**, *8*, 4544–4549. [[CrossRef](#)]
20. Inthapanya, X.; Wu, S.; Han, Z.; Zeng, G.; Wu, M.; Yang, C. Adsorptive removal of anionic dye using calcined oyster shells: Isotherms, kinetics, and thermodynamics. *Environ. Sci. Pollut. Res.* **2019**, *26*, 5944–5954. [[CrossRef](#)]
21. Faizal, A.N.M.; Putra, N.R.; Zaini, M.A.A. *Scylla* Sp. Shell: A potential green adsorbent for wastewater treatment. *Toxin Rev.* **2022**, *41*, 1280–1289. [[CrossRef](#)]
22. Londono-Zuluaga, C.; Jameel, H.; Gonzalez, R.W.; Lucia, L. Crustacean shell-based biosorption water remediation platforms: Status and perspectives. *J. Environ. Manag.* **2018**, *231*, 757–762. [[CrossRef](#)]
23. FAO—United Nations Food and Agriculture Organization. *The State of World Fisheries and Aquaculture—Towards Blue Transformation*; FAO: Rome, Italy, 2022.
24. Nekvapil, F.; Ganea, I.-V.; Ciorîță, A.; Hirian, R.; Ogresta, L.; Glamuzina, B.; Roba, C.; Pinzaru, S.C. Wasted Biomaterials from Crustaceans as a Compliant Natural Product Regarding Microbiological, Antibacterial Properties and Heavy Metal Content for Reuse in Blue Bioeconomy: A Preliminary Study. *Materials* **2021**, *14*, 4558. [[CrossRef](#)]
25. EC—European Commission. Communication from the Commission to the European Parliament, the European Council, the Council, the European Economic and Social Committee and the Committee of the Regions on The European Green Deal. COM/2019/640 final. Available online: <https://eur-lex.europa.eu/legal-content/EN/TXT/?uri=COM%3A2019%3A640%3AFIN> (accessed on 1 December 2021).
26. EC—European Commission. Communication from the Commission to the European Parliament, the European Council, the Council, the European Economic and Social Committee and the Committee of the Regions on a new approach for a sustainable blue economy in the EU: Transforming the EU’s Blue Economy for a Sustainable Future. COM/240/2021 Final. Available online: <https://eur-lex.europa.eu/legal-content/EN/TXT/?uri=COM:2021:240:FIN> (accessed on 1 December 2021).
27. EPA—United States Environmental Protection Agency. National Recycling Strategy—Part One of a Series on Building a Circular Economy for All. Available online: <https://www.epa.gov/system/files/documents/2021-11/final-national-recycling-strategy.pdf> (accessed on 19 December 2022).
28. EC—Commission of the European Communities. Green Paper on the Management of Bio-Waste in the European Union. COM(2008) 811 Final. Available online: <https://eur-lex.europa.eu/legal-content/EN/TXT/PDF/?uri=CELEX:52008DC0811&from=EN> (accessed on 19 December 2022).
29. Ogresta, L.; Nekvapil, F.; Tămaș, T.; Barbu-Tudoran, L.; Suci, M.; Hirian, R.; Aluas, M.; Lazar, G.; Levei, E.; Glamuzina, B.; et al. Rapid and Application-Tailored Assessment Tool for Biogenic Powders from Crustacean Shell Waste: Fourier Transform-Infrared Spectroscopy Complemented with X-ray Diffraction, Scanning Electron Microscopy, and Nuclear Magnetic Resonance Spectroscopy. *ACS Omega* **2021**, *6*, 27773–27780. [[CrossRef](#)]
30. Antunes-Valcareggi, S.A.; Ferreira, S.R.S.; Hense, H. Enzymatic Hydrolysis of Blue Crab (*Callinectes Sapidus*) Waste Processing to Obtain Chitin, Protein, and Astaxanthin-Enriched Extract. *Int. J. Environ. Agricult. Res.* **2017**, *3*, 81–92.
31. Montoya, J.M.; Mata, S.V.; Acosta, J.L.; Herrera Cabrera, B.E.; Lopez Valdez, L.G.; Reyes, C.; Barrales Curenio, H.J. Obtaining of Astaxanthin from Crab Exoskeletons and Shrimp Head Shells. *Biointerface Res. Appl. Chem.* **2021**, *11*, 13516–13523. [[CrossRef](#)]
32. Lindberg, D.; Solstad, R.G.; Arnesen, J.A.; Helmers, A.K.; Whitaker, R.D. Lab scale sustainable extraction of components from snow crab (*Chionoecetes opilio*) co-products, and estimation of processing costs based on a small-scale demonstration plant (Bioteq). *Ökonomisk Fisk.* **2021**, *31*, 42–57.

33. Rodrigues, L.; Pereira, C.; Leonardo, I.; Fernández, N.; Gaspar, F.; Silva, J.; Reis, R.; Duarte, A.R.C.; Paiva, A.; Matias, A. Terpene-Based Natural Deep Eutectic Systems as Efficient Solvents To Recover Astaxanthin from Brown Crab Shell Residues. *ACS Sustain. Chem Eng.* **2020**, *8*, 2246–2259. [[CrossRef](#)]
34. Nunes, A.N.; Roda, A.; Gouveia, L.F.; Fernandez, N.; Bronze, M.R.; Matias, A.A. Astaxanthin Extraction from Marine Crustacean Waste Streams: An Integrated Approach between Microwaves and Supercritical Fluids. *ACS Sustain. Chem. Eng.* **2021**, *9*, 3050–3059. [[CrossRef](#)]
35. Salares, V.R.; Young, N.M.; Bernstein, H.J.; Carey, P.R. Resonance Raman spectra of lobster shell carotenoproteins and a model astaxanthin aggregate. A possible photobiological function for the yellow protein. *Biochemistry* **1977**, *16*, 4751–4756. [[CrossRef](#)]
36. Pinzaru, S.C.; Müller, C.; Tomšić, S.; Venter, M.M.; Cozar, B.I.; Glamuzina, B. New SERS feature of  $\beta$ -carotene: Consequences for quantitative SERS analysis. *J. Raman Spectrosc.* **2015**, *46*, 597–604. [[CrossRef](#)]
37. Nekvapil, F.; Brezestean, I.; Lazar, G.; Firta, C.; Pinzaru, S.C. Resonance Raman and SERRS of fucoxanthin: Prospects for carotenoid quantification in live diatom cells. *J. Mol. Struct.* **2021**, *1250*, 131608. [[CrossRef](#)]
38. Guillen, A.D.; Cabo, N. Infrared Spectroscopy in the Study of Edible Oils and Fats. *J. Sci. Food Agric.* **1997**, *75*, 1–11. [[CrossRef](#)]
39. Thommes, M.; Kaneko, K.; Neimark, A.V.; Olivier, J.P.; Rodriguez-Reinoso, F.; Rouquerol, J.; Sing, K.S.W. Physisorption of gases, with special reference to the evaluation of surface area and pore size distribution (IUPAC Technical Report). *Pure Appl. Chem.* **2015**, *87*, 1051–1069. [[CrossRef](#)]
40. Perrin, J.; Vielzeuf, D.; Laporte, D.; Ricolleau, A.; Rossman, G.R.; Floquet, N. Raman characterization of synthetic magnesian calcites. *Am. Mineral.* **2016**, *101*, 2525–2538. [[CrossRef](#)]
41. Wysokowski, M.; Petrenko, I.; Motylenko, M.; Langer, E.; Bazhenov, V.V.; Galli, R.; Stelling, A.L.; Kljajić, Z.; Szatkowski, T.; Kutsova, V.Z.; et al. Renewable chitin from marine sponge as a thermostable biological template for hydrothermal synthesis of hematite nanospheres using principles of extreme biomimetics. *Bioinspired Mater.* **2015**, *1*, 12–22. [[CrossRef](#)]
42. Andersen, F.A.; Brecevic, L.; Beuter, G.; Dell’Amico, D.B.; Calderazzo, F.; Bjerrum, N.J.; Underhill, A.E. Infrared Spectra of Amorphous and Crystalline Calcium Carbonate. *Acta Chem. Scand.* **1991**, *45*, 1018–1024. [[CrossRef](#)]
43. Lavall, R.L.; Assis, O.B.G.; Campana-Filho, S.P.  $\beta$ -Chitin from the pens of *Loligo* sp.: Extraction and characterization. *Bioresour. Technol.* **2007**, *98*, 2465–2472. [[CrossRef](#)]
44. Coleyshaw, E.E.; Crump, G.; Griffith, W.P. Vibrational spectra of the hydrated carbonate minerals ikaite, monohydrocalcite, lansfordite and nesquehonite. *Spectrochim. Acta Part A Mol. Biomol. Spectrosc.* **2003**, *59*, 2231–2239. [[CrossRef](#)]
45. Dotto, G.L.; McKay, G. Current scenario and challenges in adsorption for water treatment. *J. Environ. Chem. Eng.* **2020**, *8*, 103988. [[CrossRef](#)]
46. Yao, H.; Zheng, G.; Li, W.; McDowell, M.T.; Seh, Z.W.; Liu, N.; Lu, Z.; Cui, Y. Crab Shells as Sustainable Templates from Nature for Nanostructured Battery Electrodes. *Nano Lett.* **2013**, *13*, 3385–3390. [[CrossRef](#)]
47. Fortune Business Insights. Carotenoids Market Size, Share & COVID-19 Impact Analysis, By Type (Astaxanthin, Beta-Carotene, Lutein, Zeaxanthin, Lycopene, Canthaxanthin, and others), Source (Synthetic and Natural), Application (Animal Feed, Food & Beverages, Dietary Supplements, Personal Care & Cosmetics, and Pharmaceuti-cals), and Regional Forecast 2020–2027. Available online: <https://www.fortunebusinessinsights.com/industry-reports/carotenoids-market-100180> (accessed on 3 January 2023).

**Disclaimer/Publisher’s Note:** The statements, opinions and data contained in all publications are solely those of the individual author(s) and contributor(s) and not of MDPI and/or the editor(s). MDPI and/or the editor(s) disclaim responsibility for any injury to people or property resulting from any ideas, methods, instructions or products referred to in the content.